Adaptive Fuzzy Superpixels for Polarimetric SAR Images Classification

Yuwei Guo, *Member, IEEE,* Licheng Jiao, *Fellow, IEEE,* Rong Qu, *Senior Member, IEEE,* Shuang Wang, *Member, IEEE,* Shuo Wang, *Member, IEEE,* Fang Liu, *Senior Member, IEEE* and Zhuangzhuang Sun

***Abstract*—The increasing applications of Polarimetric SAR (PolSAR) image classification demand for effective superpixels algorithms. Fuzzy superpixels algorithms reduce the misclassification rate by dividing pixels into superpixels, which are groups of pixels of homogenous appearance, and undetermined pixels. However, two key issues remain to be addressed in designing a fuzzy superpixel algorithm for PolSAR image classification. Firstly, the polarimetric scattering information, which is unique in PolSAR images, is not effectively used. Such information can be utilized to generate superpixels more suitable for PolSAR images. Secondly, the ratio of undetermined pixels is fixed for each image in the existing techniques, ignoring the fact that the difficulty of classifying different objects varies in an image. To address these two issues, we propose a polarimetric scattering information based adaptive fuzzy superpixels (AFS) algorithm for PolSAR images classification. In AFS, the correlation between pixels' polarimetric scattering information, for the first time, is considered to generate superpixels. This correlation is further used to dynamically and adaptively update the ratio of undetermined pixels. AFS is evaluated extensively against different evaluation metrics and compared with the state-of-the-art superpixels algorithms on three PolSAR images. The experimental results demonstrate the superiority of AFS on PolSAR image classification problems.**

***Index Terms*—fuzzy superpixels, fuzzy rough set, polarimetric synthetic aperture radar (PolSAR), image classification**

I. INTRODUCTION

Superpixels algorithms segment an image into smaller regions named superpixels with homogenous appearance and common characteristics [1]. By preserving the spatial neighborhood information, superpixels algorithms with improved computational efficiency have been widely applied in computer vision. Applications include image classification [2]-[5], segmentation [6]-[8], image enhancement [9], foreground extraction [10]-[12] and visual object tracking [13]-[15].

Remote sensing image classification has attracted a lot of research attention in recent years [16], [17]. Among the developments of polarimetric synthetic aperture radar (PolSAR), PolSAR image classification becomes an important research topic in remote sensing image classification. With the ability to suppress speckle noises of PolSAR image and improve the computation efficiency, superpixels algorithms have been widely investigated in PolSAR classification [18]–[20].

Due to their versatility, superpixels algorithms are often used as a general preprocessing method, applicable to any image applications. However, the underlying nature of different applications is often neglected in generating superpixels. Domain specific information should be considered in designing superpixels algorithms to improve PolSAR image classification.

An assumption in superpixels-based classification algorithms is that all the pixels in any single superpixel belong to the same class, i.e. defined as *pure superpixels*. Superpixels consisting of pixels of different classes are defined as *mixed superpixels*. In practical applications, it is believed that both pure superpixels and mixed superpixels exist [21]. Mixed superpixels lead to misclassifications regardless of which classification method is used [22].

Fuzzy superpixels algorithms become popular for PolSAR image classification in recent years. By segmenting pixels into superpixels and undetermined pixels, they reduce the generation of mixed superpixels and misclassification rate. Pixels which are hard to classify are defined as *undetermined pixels*. In the existing fuzzy superpixels algorithms, the ratio of undetermined pixels over all pixels is fixed in each image. However, the difficulty of distinguishing objects in an image varies. For example, it is much easier to distinguish between waters and towns than to distinguish between forests and towns. The ratio of undetermined pixels in an image should be adjusted adaptively in fuzzy superpixels algorithms.

In designing a superpixels algorithm suitable for PolSAR image, the unique polarimetric scattering information by polarimetric imaging [23] should also be effectively used. In PolSAR imaging, some factors, such as Doppler parameters, range migration, speckle noise and object azimuth angle, can lead to uncertainty and inconsistency [24]. An algorithm capable of handling uncertain and inconsistent data is thus needed by utilizing polarimetric scattering information effectively.

To address the above issues, we propose a polarimetric scattering information based Adaptive Fuzzy Superpixels (AFS) algorithm for PolSAR image classification. By adapting the ideas in clustering technologies, AFS integrates polarimetric scattering information, color information and position information to generate fuzzy superpixels. As an efficient tool for mining knowledge from uncertain and inconsistent data [25]–[27], the fuzzy rough set theory is used in AFS to measure the correlation between polarimetric scattering information of PolSAR data. The ratio of undetermined pixels is adjusted adaptively by the calculated correlation. The main contributions of this research can be summarized as follows.

- The unique characteristic of polarimetric scattering information in PolSAR images is introduced to generate improved fuzzy superpixels suitable for PolSAR image.
- The correlation between polarimetric scattering information is, for the first time, measured effectively by fuzzy rough set theory to enhance fuzzy superpixels algorithms.
- The ratio of undetermined pixels is adaptively adjusted according to the correlation between polarimetric scattering information to produce adaptive fuzzy superpixels.

The remainder of this paper is organized as follows. Section II reviews the superpixels and fuzzy superpixels algorithms. The proposed AFS algorithm is presented in Section III. Section IV presents and analyses the experimental results. We conclude this work and plan for the future research in Section V.

II. RELATED WORKS

In this section, we briefly review representative superpixels and fuzzy superpixels algorithms in the existing literature.

Ncut. Ncut [28] extracts the global impression of an image. It partitions the image by using graph-theoretic criterion to compute the cut cost, i.e. fraction of the total edge connections to all the nodes in the graph. Ncut produces more regular and compact superpixels but is usually time-consuming.

SLIC. SLIC uses the k-means clustering algorithm to produce superpixels [29]. The distance measure in SLIC combines color and spatial proximity. The compactness and the number of superpixels can be controlled flexibly. Due to its simplicity, SLIC has been widely used in image processing.

LSC. In LSC [30], both the color similarity and space proximity are measured based on normalized cuts. The cost function of the normalized cuts is optimized by iteratively using k-means clustering. Therefore, LSC has a low linear computational complexity and high memory efficiency.

IMSLIC. Extended from SLIC, IMSLIC [31] produces content-sensitive superpixels. The original image is mapped to a two-dimensional manifold. The content sensitivity measures Voronoi cells areas in the manifold. An easy and quick approximation is executed to reduce computational complexity.

USEAQ. USEAQ [32] performs joint spatial and color quantization to group pixels into regions. The difference between regions is then considered to adaptively select one or several superpixel candidates for each region. Finally, pixels are assigned to superpixels by maximizing a posteriori estimation. The algorithm reduces the computational cost of iterative optimization procedures by using a one-pass method.

LearnedS. LearnedS [33] aims to learn pixel affinities. A proposed segmentation-aware loss makes use of segmentation errors to learn affinities for superpixel segmentation. The algorithm generates better boundary-preserving superpixels compared to those using hand-crafted features.

FS. FS is first proposed in 2018 for image classification [34]. To ensure that pixels in the same superpixel belong to the same class as much as possible, the FS algorithm divides an image into superpixels and undetermined pixels. FS is based on the fuzzy c-means clustering algorithm, which uses color and spatial information to cluster pixels.

III. ADAPTIVE FUZZY SUPERPIXELS BASED ON POLARIMETRIC SCATTERING INFORMATION

In this section, features of the polarimetric scattering information of pixels in PolSAR images are firstly explained. Secondly, we calculate the correlation between these features by fuzzy rough set theory. Thirdly, fuzzy superpixels in the AFS algorithm are initialized with the color information, the position information and the polarimetric scattering information represented by these features. Next, the ratio of undetermined pixels in fuzzy superpixels is determined adaptively by the calculated correlation between these features. Finally, we present the post-processing.

A. Feature representation of polarimetric scattering information

PolSAR transmits and receives signals in various combinations of polarization. The obtained PolSAR image with diverse polarization combinations thus contains more detailed scattering information than that in optical images and traditional SAR images [35].

Polarimetric scattering information is unique to PolSAR images. Each pixel in a PolSAR image is represented by a coherency matrix T, which contains fully polarimetric scattering information and retains second-order statistics of polarimetric scattering information, as shown in Formula (1):

$$T = \begin{bmatrix} T_{11} & T_{12} & T_{13} \\ T_{12}^{*} & T_{22} & T_{23} \\ T_{13}^{*} & T_{23}^{*} & T_{33} \end{bmatrix} \tag{1}$$

To avoid complex calculations, the real part and imaginary part of the elements in T are separated to represent the polarimetric scattering information of each pixel as a feature vector. The feature vector of the i^{th} pixel is defined in Formula (2).

$$\begin{aligned} fea_i &= \left[f_{i1}, f_{i2}, ..., f_{i9} \right] \\ &= \left[T_{i11}, T_{i22}, T_{i33}, real(T_{i12}), imag(T_{i12}), real(T_{i13}), imag(T_{i13}), real(T_{i23}), imag(T_{i23}) \right] \end{aligned} \tag{2}$$

B. Correlation between polarimetric scattering information

Fuzzy rough set theory [26] combines roughness with vagueness. Fuzzy equiva¬lence relation, which is key to fuzzy rough set theory, is usually used to measure the correlation between samples [27]. In the proposed AFS, we use fuzzy equivalence relation to measure the correlation between the polarimetric scattering information of pixels. Given a non-empty finite samples set $X = [x_1,\ldots,x_i,\ldots,x_j,\ldots,x_n]$, x_i represents the i^{th} pixel of a PolSAR image. The fuzzy equivalence relation $\tilde{R}$ can be defined on X if $\tilde{R}$ satisfies reflectivity, symmetry and transitivity, shown in Formula (3).

$$\tilde{R} = \begin{pmatrix} r_{11} & r_{12} & \ldots & r_{1n} \\ r_{21} & r_{22} & \ldots & r_{2n} \\ \ldots & \ldots & r_{ij} & \ldots \\ r_{n1} & r_{n2} & \ldots & r_{nn} \end{pmatrix} \tag{3}$$

where, r_{ij} is the fuzzy equivalence relation value between the i^{th} and j^{th} pixels.

Using the same technique in [27], r_{ij} is computed by the similarity function defined in Formula (4).

$$r_{ij} = \begin{cases} 1 - 4 \times \dfrac{\left| f_{it} - f_{jt} \right|}{\left| f_{t\max} - f_{t\min} \right|}, \dfrac{\left| f_{it} - f_{jt} \right|}{\left| f_{t\max} - f_{t\min} \right|} \le 0.25 \\ 0, otherwise \end{cases} \tag{4}$$

where f_{it}, f_{jt} is the feature value of the i^{th} and j^{th} pixels for feature t, respectively. $t = [1,2,\ldots,9]$. f_{tmax} and f_{tmin} is the maximal and minimal value of feature t, respectively. r_{ij} thus represents the correlation between pixels. The larger the value r_{ij} is, the more correlated the two pixels are.

C. Polarimetric scattering information based fuzzy superpixels

By using the fuzzy equivalence relation $\tilde{R}$, the calculated correlation between pixels' polarimetric scattering information is introduced to generate fuzzy superpixels in the proposed AFS algorithm.

1) Initialize pixels clustering: Like in [29] and [34], with the desired number of fuzzy superpixels K, K cluster centers are selected on a regular grid space $S = N / K$, N is the total number of pixels in an image. To avoid cluster centers on an edge or a noisy pixel, the centers are moved to a position of the lowest gradient in a 3×3 neighborhood. For each center, the size of the search region for finding pixels belonging to the same class is set to 2S×2S. With the initial cluster centers and the size of search region, the non-overlapping search region and overlapping search region are determined [34]. The overlapping search region consists of pixels of different cluster centers. The non-overlapping search region contains pixels corresponding to only one cluster center.

An example of overlapping and non-overlapping search regions is given in Fig. 1. Among the 25 pixels, assume pixels 4, 7 and 18 are cluster centers. Within the search region of 3×3, pixel 1 belongs to only the center pixel 7, thus is in a non-overlapping search region. Pixel 12 belongs to two search regions corresponding to center pixels 7 and 18, thus is in an overlapping search region. In Fig. 1, there are two overlapping search regions, i.e. one consists of pixels 3 and 8, and the other consists of pixels 12 and 13.

Fig. 1. An example of overlapping and non-overlapping search regions.

2) Pixels clustering for superpixels: Following the same idea of clustering, superpixels algorithms group a set of pixels, i.e. a superpixel, which are more similar to each other in some sense than to those in other superpixels. Clustering models differ significantly based on what constitutes a superpixel and how to find them efficiently.

The pixels in the non-overlapping region have the same label as that of the corresponding cluster centers. For a pixel in an overlapping region, a new objective function based on the widely used fuzzy c-means clustering (FCM) defined in Formula (5) is proposed in Formula (6) to determine which superpixel it belongs to.

The classical FCM algorithm is a simple fuzzy clustering algorithm [36], where each data point may belong to more than one cluster with different membership values ranging from [0,1], the sum of which for each data point must be one. Let $X = [x_1,x_2,\ldots,x_i,\ldots,x_N]$, be a data set of N pixels in a Z-dimensional Euclidean space ($x_i \in R^Z$). Clustering is a process which partitions the data set into C subsets, cluster centers of which are $V = [v_1,v_2,\ldots,v_j,\ldots,v_C]$. The FCM algorithm minimizes the objective function in Formula (5), which is the generalized form of the least-squared errors function [37].

$$J_m(U,C) = \sum_{j=1}^{C}\sum_{i=1}^{N} u_{ij}^m D_{ij}^2 \qquad s.t. \sum_{j=1}^{C} u_{ij} = 1 \tag{5}$$

where m is the weighting fuzziness parameter and is usually set as 2. u_{ij} is the membership value of the i^{th} data point to the m cluster center.

A new objective function in Formula (6) is devised in AFS to redefine the distance D_{ij} in Formula (5).

$$J_{new}(U,C) = \sum_{j=1}^{C}\sum_{i=1}^{N} u_{ij}^m D_{new_{ij}}^2 \qquad s.t. \sum_{j=1}^{C} u_{ij} = 1 \tag{6}$$

where the new distance measure $D_{new_{ij}}$ is defined in Formula (7). The parameter φ sets a tradeoff weighting between all the information, and is determined by experimental analysis, see Section IV. C.

$$D_{new_{ij}} = dc_{ij} + dp_{ij} + \varphi(1 - r_{ij}) \tag{7}$$

The new distance $D_{new_{ij}}$ considers the information of the color as defined in Formula (8), the position as defined in Formula (9), and the polarimetric scattering in Formula (4). The underlying idea is threefold. Firstly, pixels with the same RGB value are more similar to each other. Secondly, pixels are more similar to nearby pixels than those farther away. Thirdly, pixels with correlative polarimetric scattering information are more similar than those with different scattering information.

In the proposed AFS, the color information is extracted from the Pauli-color coding image. For visualization purpose, it is a common practice to generate pseudo color images by mapping backscattering elements to different color channels, e.g. the Pauli-color coding image [38]. The color of a pixel is represented in the CIELAB color space $[l,a,b]^T$. The distance in terms of color information dc_{ij} as defined in Formula (8) is measured by the Euclidean distance between the color of the i^{th} pixel and the j^t cluster center pixel.

$$dc_{ij} = \sqrt{(l_i - l_j)^2 + (a_i - a_j)^2 + (b_i - b_j)^2} \tag{8}$$

The position information is the coordinates of pixels, represented as $[px,py]$. The distance in terms of position information dp_{ij} as defined in Formula (9) is computed by the Euclidean distance between the coordinate of i^{th} pixel and the coordinate of the j^{th} cluster center pixel.

$$dp_{ij} = \sqrt{(px_i - px_j)^2 + (py_i - py_j)^2} \tag{9}$$

The distance in terms of polarimetric scattering information is represented by $(1–r_{ij})$, see Section III-B, as a consistent distance measure.

The Lagrangian multiplier method [39] can be used to solve the minimization problem in Formula (6), i.e. Formula (10) and (11) are used to change the degree of membership of each data point and cluster center in each iteration.

$$u_{ij}^m = \left[\sum_{k=1}^{C} \left(\frac{D_{new_{ij}}}{D_{new_{ik}}} \right)^{\frac{2}{m-1}} \right]^{-1} \tag{10}$$

$$v_j = \frac{\sum_{i=1}^{N} u_{ij}^m x_i}{\sum_{i=1}^{N} u_{ij}^m} \tag{11}$$

D. Adaptive ratio of undetermined pixels

The proposed AFS algorithm divides the pixels of an image into superpixels and undetermined pixels. In most of the literature [34], the ratio of undetermined pixels to all pixels is fixed to 0.5. In AFS, with an initial value of 0.5, the ratio of undetermined pixels as defined in Formula (12) is adjusted adaptively according to the difference between the correlation of pixels in the same and different classes as defined in Formula (13).

$$P_{un} = 0.5 \times \frac{1}{RelDiff} \quad and \quad P_{un} < 1 \tag{12}$$

$$RelDiff = \frac{1}{C(C-1)}\left[C \times \text{sum}(\text{diag}(Rel)) - \text{sum}(Rel)\right] \tag{13}$$

The definition of *RelDiff* in (13) follows the idea of clustering, that pixels in the same class are expected to be more correlated to each other than to those in other classes. The first term in brackets represents the sum of the correlation values of pixels in the same class. The second term is the sum of all the correlation values. Higher *RelDiff* means that pixels in the same class are more correlaed to each other, and pixels in different classes are less correlated to each other. *Rel* is the correlation matrix between pixels belonging to the same and different classes, as defined in Formula (14).

$$Rel = U^T \tilde{R} U = \begin{bmatrix} Rel_{11} & Rel_{12} & & Rel_{1C} \\ Rel_{21} & Rel_{22} & & Rel_{2C} \\ & & Rel_{tq} & \\ Rel_{C1} & Rel_{C2} & & Rel_{CC} \end{bmatrix} \tag{14}$$

where *Rel* is a symmetric matrix, *U* is the membership matrix computed by Formula (10) and $\tilde{R}$ is the correlation matrix computed by Formula (3). Rel_{tq} is the correlation value between the pixels in the t^{th} class and the pixels in the q^{th} class.

E. Post-processing

To enforce region connectivity, a post-processing step is adopted at the end of the clustering procedure. For superpixels in fuzzy superpixels, similar to the post-processing in [29], small superpixels are assigned the label of the nearest superpixels. Note that we ignore the undetermined pixels when merging small regions. For each undetermined pixel *up*, the number of superpixels Num_s in the $M \times M$ region centered with *up* is computed. If $Num_s > 1$, then pixels in the region are redefined as undetermined pixels. If $Num_s=1$, the undetermined pixel is assigned the same label as that of the other pixels in the region. The size of the search region is set to 9×9 in our experiments.

F. Procedure of the AFS Algorithm

The proposed fuzzy equivalence relation based fuzzy-superpixels (AFS) algorithm is summarized in Algorithm 1.

Algorithm 1: Adaptive Fuzzy Superpixels (AFS)

Input: the number of superpixels *K*, the threshold *epsilon*, the number of iterations *itmax*, the weighting parameter φ

Output: fuzzy-superpixels

Step1: Initialize cluster centers and find out non-overlapping and overlapping search regions. // Section III-C 1).

Step2: Identify pixels in each non-overlapping search region which belong to the superpixels of the corresponding cluster centers. // Section III-C 2)

Step3: Measure the membership degree between the pixels and center pixels using Formula (10).

Step4: For pixels in each overlapping search region, compute the corresponding cluster centers using Formula (11).
Step5: Determine the ratio of the undetermined pixels using Formula (12).
Step6: Repeat Steps 3 to 5 until reaching *itmax* or the difference between cluster centers in two iterations is less than *epsilon*.
Step7: Post-processing. // Section III-E

IV. EXPERIMENTAL ANALYSIS AND RESULT

A. Data Sets

The following three frequently used PolSAR images have been selected to evaluate the performance and effectiveness of the proposed AFS algorithm quantitatively and qualitatively.

- Flevoland image (300×270 pixels): was caught by AIRSAR airborne platform on an area in Flevoland, the Netherlands. There are many kinds of natural areas in Flevoland, such as bare soil, potatoes, beet and so on.
- ESAR image (1300×1200 pixels): is an L-band multilook PolSAR image taken by the E-SAR at the German Aerospace Center. The scene covers Oberpfaffenhofen, Germany. Besides natural areas, there are also a lot of building areas.
- San Francisco image (1300×1300 pixels): covers the area around Bay of San Francisco with the golden gate bridge, with both natural and man-made areas.

Fig. 2(a), 3(a) and 4(a) shows the three false color images acquired by Pauli decomposition [38], respectively. Fig. 2(b) and Fig. 2(c) shows the ground truth map [40] and the color codes representing the classes for Flevoland, respectively. The Flevoland image is segmented into six classes. The ground truth map for ESAR is acquired by [41], as shown in Fig. 3(b), with three classes including built-up areas, wood land and open areas, as shown by the color code in Fig. 3(c). The ground truth map for San Francisco is shown in Fig. 4(b) [42], and Fig. 4(c) shows the corresponding color code of five classes: low-density urban, water, vegetation, high-density urban and developed. Note that pixels in the void regions are not labeled. Labelling PolSAR images is highly labor-intensive and time-consuming [43]-[45], thus void regions are very common in ground truth of PolSAR images.

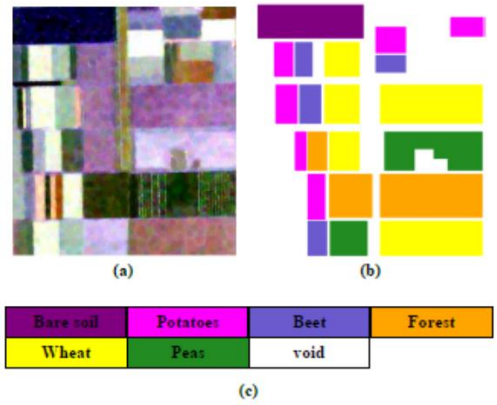

Fig. 2. Flevoland. (a) PolSAR image (PauliRGB). (b) The ground truth map. (c) Color code.

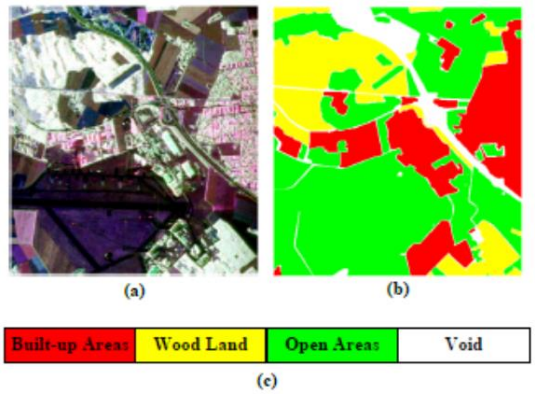

Fig. 3. Esar. (a) PolSAR image (PauliRGB). (b) The ground truth map. (c) Color code.

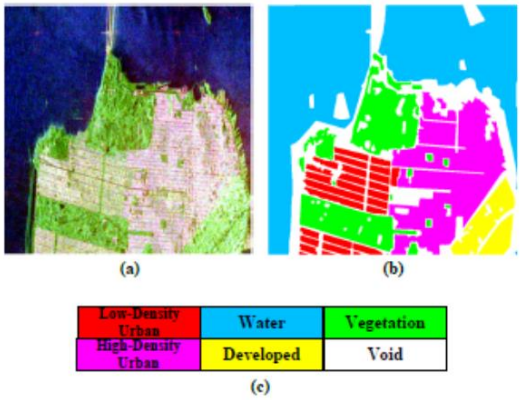

Fig. 4. SanFrancisco. (a) PolSAR image (PauliRGB). (b) The ground truth map. (c) Color code.

B. Effectiveness of polarimetric scattering information

For each pixel, the polarimetric scattering information represented in a feature vector as shown in Formula (2). The correlation of polarimetric scattering information between pixels is calculated by using fuzzy rough set theory as explained in Sec. III-B. The effectiveness of xxx is demonstrated in the following two experiments to show if the correlation between pixels can indicate if the pixels have the same label. In the first experiment, the correlation is calculated between pixels randomly selected from the entire image. In the second experiment, a region is randomly picked from the image, and the correlation between pixels in the selected region is computed.

1) Experimental analysis on pixels selected at random:

For each PolSAR image, ten pixels are randomly selected from each class, respectively. Note that, based on experiments, only the first three features (i.e. the values on the diagonal of the coherency matrix in Formula (1)) are used to compute the correlation between pixels. Table I, II and III shows the correlation between the randomly selected pixels in Flevoland, ESAR and San Francisco, respectively. The elements on the diagonal are the correlations between pixels belonging to the corresponding same class. The other values represent the correlations between pixels with different labels. For example, the value “0.0908” in the second row and the first column in Table I is the average correlation between pixels belonging to class 2 and pixels belonging to class 1. As shown in Tables I to III, the values on the diagonal are the largest, showing that pixels belonging to the same class have a higher correlation than those belonging

to different classes. The experiment indicates that the correlation of scattering information of pixels can be effectively evaluated by the fuzzy rough set theory. The correlation thus can be used to cluster pixels for generating fuzzy superpixels.

TABLE I
FLEVOLAND. THE AVERAGE CORRELATION OF THE SCATTERING INFORMATION BETWEEN RANDOMLY SELECTED PIXELS.

Class	1	2	3	4	5	6
1	**0.8760**	0.0908	0	0.3788	0.7773	0.00008
2	0.0908	**0.4514**	0.3130	0.0314	0.0761	0.1819
3	0	0.3130	**0.7837**	0.0021	0	0.2809
4	0.3788	0.0314	0.0021	**0.8952**	0.4817	0.0095
5	0.7773	0.0761	0	0.4817	**0.9342**	0.0001
6	0.00008	0.1819	0.2809	0.0095	0.0001	**0.8433**

TABLE II
ESAR. THE AVERAGE CORRELATION OF SCATTERING INFORMATION BETWEEN RANDOMLY SELECTED PIXELS.

Class	1	2	3
1	**0.3681**	0.1652	0.1418
2	0.1652	**0.9015**	0.6167
3	0.1418	0.6167	**0.9519**

TABLE III
SAN FRANCISCO. THE AVERAGE CORRELATION OF SCATTERING INFORMATION BETWEEN RANDOMLY SELECTED PIXELS .

Class	1	2	3	4	5
1	**0.9899**	0.8519	0.6288	0.2969	0.0085
2	0.8519	**0.9305**	0.6794	0.3249	0.0048
3	0.6288	0.6794	**0.9429**	0.3520	0.0474
4	0.2969	0.3249	0.3520	**0.5672**	0.1639
5	0.0085	0.0048	0.0474	0.1639	**0.4851**

2) Experimental analysis on regions selected at random:
Small regions with different classes of pixels are chosen randomly from the original images to analyze the correlation between pixels in the chosen regions. Fig. 5(a) shows the ground truth map of Flevoland and a selected region (indicated by the blue box). The enlarged image of the selected region is shown in Fig. 5(b). Table IV shows that the average correlation between pixels on the diagonal is even larger. It means pixels belonging to the same class have a higher correlation than those belonging to different classes. The performance of fuzzy superpixels can be improved using the correlation of scattering information between pixels.

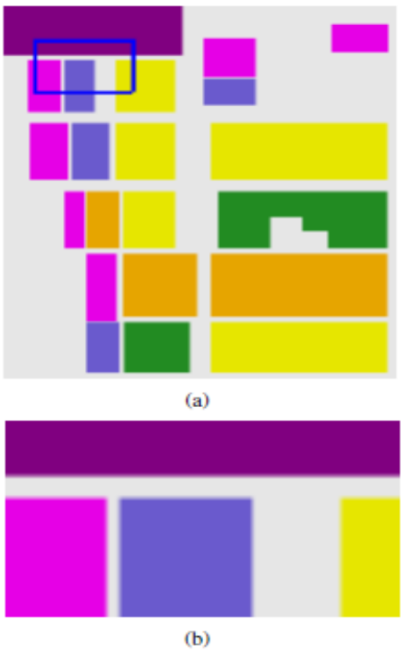

Fig. 5. Flevoland. (a) A selected region. (b) The enlarged image of the selected region with four types of terrains.

TABLE IV

FLEVOLAND. THE AVERAGE CORRELATION OF THE SCTEERING INFORMATION BETWEEN PIXELS IN A REGION.

Class	1	2	3	4
1	**0.9477**	0.0418	0.0262	0.3564
2	0.0418	**0.5350**	0.1229	0.0246
3	0.0262	0.1229	**0.5514**	0.3069
4	0.3564	0.0246	0.3069	**0.8504**

Fig. 6(a) and (b) presents the ground truth map of ESAR and the enlarged selected region with three terrains, respectively. The average correlation between pixels shown in Table V also indicates that pixels with the same label have much higher correlations than pixels with different labels.

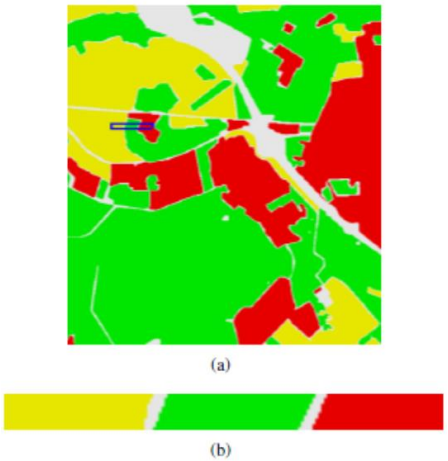

Fig. 6. ESAR. (a) A selected region. (b) The enlarged image of the selected region with three types of terrains.

TABLE V

ESAR. THE AVERAGE CORRELATION OF THE SCTEERING INFORMATION BETWEEN PIXELS IN A REGION.

Class	1	2	3
1	**0.4149**	0.1351	0.2515
2	0.1351	**0.4259**	0.0009
3	0.2515	0.0009	0.9365

Five regions are selected from the ground truth map of San Francisco, shown with blue boxes in Fig. 7(a) and enlarged in Fig. 7(b). The correlation of two terrains in each region is listed in Table VI, from which the same conclusion can be drawn.

Fig. 7. (a) San Francisco. (b) The enlarged regions each with two types of terrains.

TABLE VI

SAN FRANCISCO. THE AVERAGE CORRELATION OF THE SCTEERING INFORMATION BETWEEN PIXELS IN EACH REGION.

	Reg1		Reg2		Reg3		Reg4		Reg5	
Class	1	2	1	2	1	2	1	2	1	2
1	**0.8861**	0.2539	**0.9051**	0.6503	**0.9538**	0.7219	**0.9903**	0.6613	**0.5791**	0.4786
2	0.2539	**0.4874**	0.6503	**0.7388**	0.7219	**0.8030**	0.6614	**0.7862**	0.4786	**0.7493**

C. Analysis on parameter settings

The weighting parameter φ in the proposed AFS sets a tradeoff between color information, position information and the correlation between scattering information of pixels. The effect of the weighting parameter is shown in Fig. 8, where φ is changed from 0 to 1 with a step size of 0.2, for different number of superpixels. When φ=0, the correlation between scattering information is not considered in AFS, i.e. only the color and position information are considered. These results suggest that compared with the results without correlation (φ=0), the introduction of correlation between pixels improves the ratio of pure superpixels, with a positive effect on the performance of superpixels.

For Flevoland with 200 superpixels, when φ is 0.5 to 0.7, a higher PSR can be obtained. For Flevoland with 500 superpixels, better results are obtained when φ is 0.4 to 0.6. Thus, for Flevoland, the φ is set to 0.6. For ESAR with 500, 1000 and 3000 superpixels, when φ is 0.4, a higher PSR is obtained. Thus φ is set to 0.4 for ESAR. For San Francisco with 500 and 1000 superpixels, PSR is higher when φ is 0.2. For San Francisco with 3000 superpixels, φ is 0.4 to 0.6.

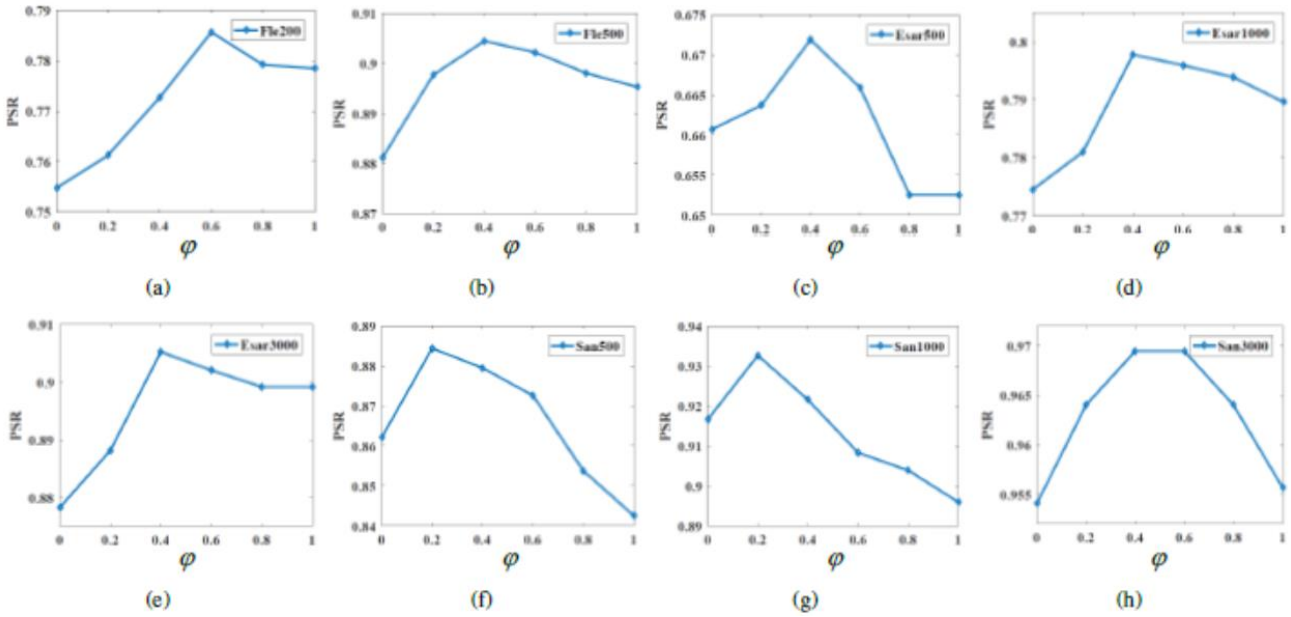

Fig. 8. PSR with different settings of the weighting parameter φ. (a) and (b): Flevoland with 200 and 500 superpixels, respectively. (c)-(e): Esar with 500, 1000 and 3000 superpixels, respectively. (f)-(h): San Francisco with 500, 1000 and 3000 superpixels, respectively.

D. In-depth comparisons with other state-of-the-art algorithms

In this section, firstly, we compare the performance of AFS against the five superpixel generation algorithms using three metrics. Secondly, the segmentation results of superpixels are visually displayed. Thirdly, a simple superpixels-based classification algorithm is utilized to demonstrate the performance of the proposed AFS. The compared algorithms include SLIC [29], LSC [30], USEAQ [32], LearnedS [33] and FS [34].

1) Performance evaluation with different metrics:

Undersegmentation Error (UE) measures the percentage of pixels overlapping with the real edges. A higher UE value indicates that the superpixels do not overlap well with the objects in the image, thus worse performance of superpixels. Based on the ground truth maps of the three PolSAR images, the UE curves of various number of superpixels are plotted in Fig. 9. PSR evaluates the ability of superpixels algorithms to generate pure superpixels. High PSR indicates that more pure superpixels are generated, thus better performance of the superpixels algorithm. Fig. 10 presents the PSR values of the six supeprixels algorithms under comparison with different number of superpixels. Fig. 9 and Fig. 10 indicate that superpixels generated by AFS are more consistent internally, i.e. pixels in a superpixel are more likely to belong to the same category.

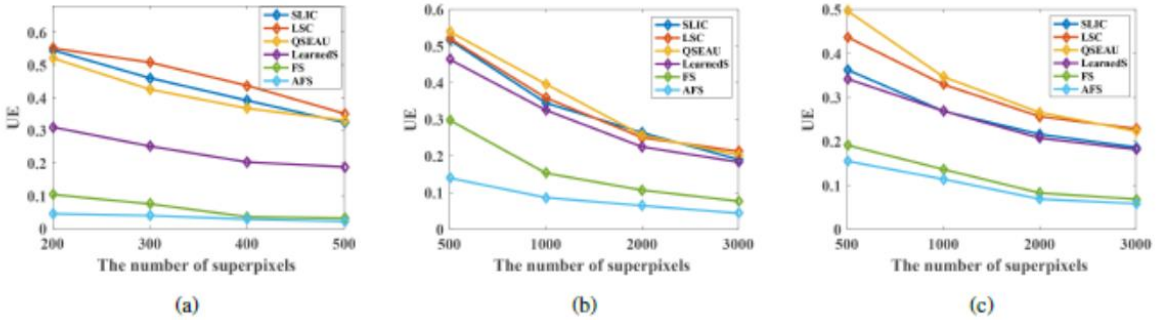

Fig. 9. Undersegmentation Error (UE). (a) Flevoland. (b) ESAR. (c) San Francisco.

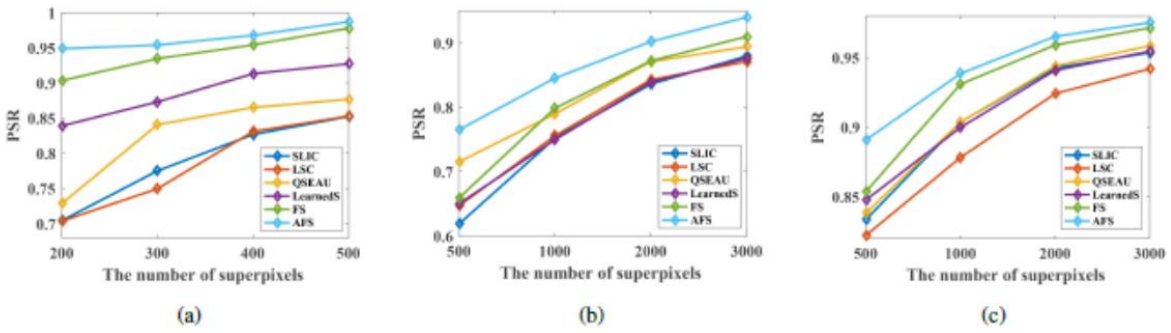

Fig. 10. Pure Superpixel Ratio (PSR). (a) Flevoland. (b) ESAR. (c) San Francisco.

The boundary adherence can be evaluated by boundary recall (BR), which computes the percentage of the real edges falling within a certain distance from a superpixel boundary [46]. The distance is usually set to 2, i.e. a two-pixel distance error. The higher the BR is, the few real edges are missed, i.e., a better boundary adherence. Using the ground truth maps, we calculate the BR values of the fuzzy superpixels algorithm FS [34] and AFS as shown in Fig. 11. FS has a better boundary adherence than AFS. This indicates that compared with FS, AFS sacrifices boundary adherence to generate more pure superpixels for classification.

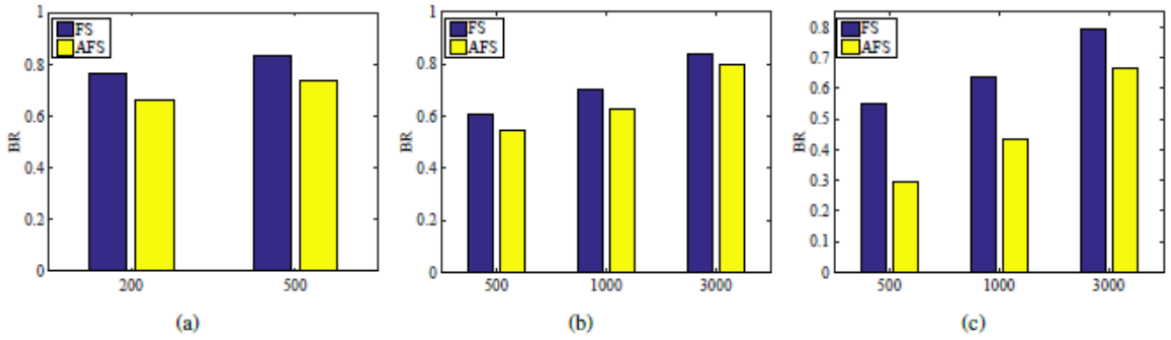

Fig. 11. Boundary Recall (BR). (a) Flevoland. (b) ESAR. (c) San Francisco.

2) Superpixels visual display:

Fig. 12 presents the superpixels segmentations of Flevoland with 200 superpixels. The enlarged superpixels segmentations of the selected area (marked with blue boxes in Fig. 12) are shown in Fig. 13. It can be seen that less superpixels generated by AFS cover two or more terrains, indicating that AFS can generate more pure superpixels. In addition, the distance between superpixels by AFS is larger than that by FS. This is because the ratio of undetermined pixels is determined adaptively in AFS according to the correlation between pixels. Fig. 14 to Fig. 19 show the superpixels segmentations and enlarged images of selected areas in ESAR and San Francisco. The number of generated superpixels is set to 500. The visual displays of superpixels lead to the same conclusion, that pixels in superpixels generated by AFS are more likely to have the same label.

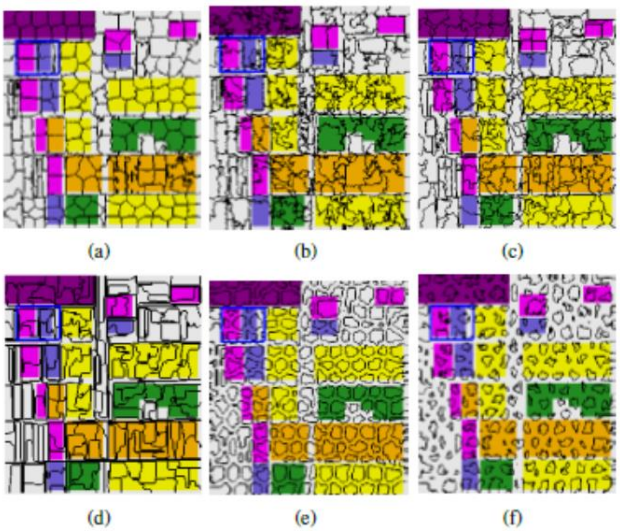

Fig. 12. Comparison of the superpixels segmentations for Flevoland using various methods. (a) SLIC. (b) LSC. (c) USEAQ. (d) LearnedS. (e) FS. (f) AFS.

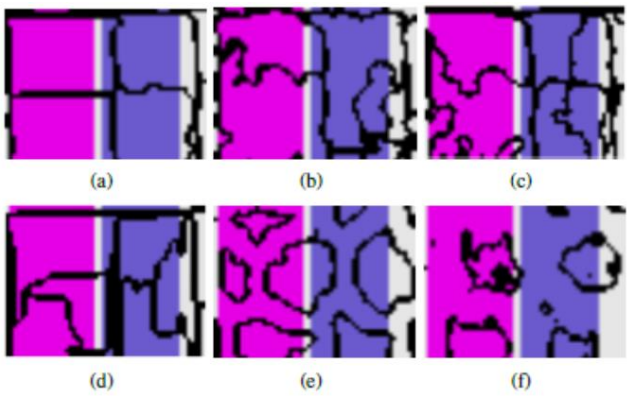

Fig. 13. The enlarged superpixels segmentations of the selected area in Flevoland. (a) SLIC. (b) LSC. (c) USEAQ. (d) LearnedS. (e) FS. (f) AFS.

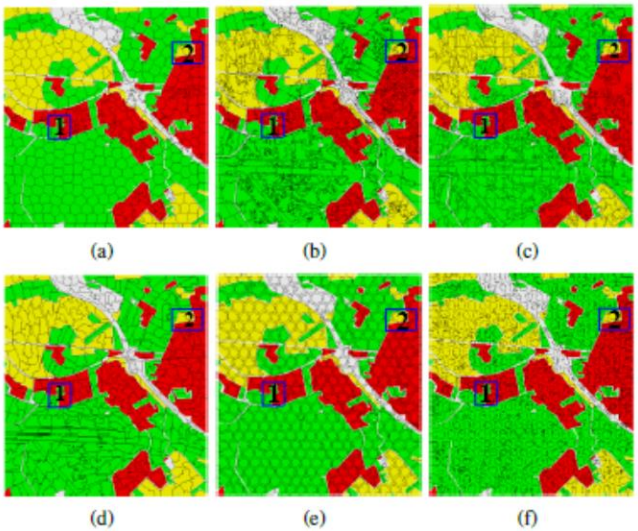

Fig. 14. Comparison of the superpixels segmentations for ESAR using various methods. (a) SLIC. (b) LSC. (c) USEAQ. (d) LearnedS. (e) FS. (f) AFS.

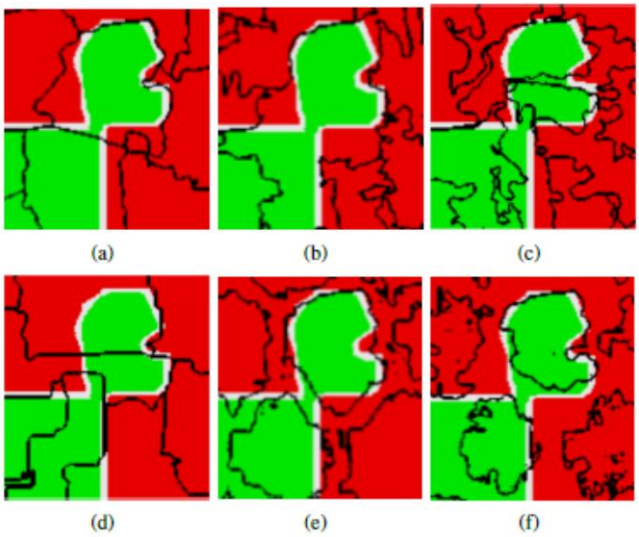

Fig. 15. The enlarged superpixels segmentations of the selected area 1 in ESAR. (a) SLIC. (b) LSC. (c) USEAQ. (d) LearnedS. (e) FS. (f) AFS.

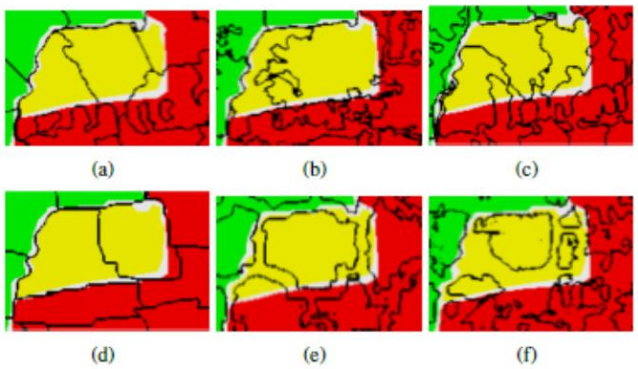

Fig. 16. The enlarged superpixels segmentations of the selected area 2 in ESAR. (a) SLIC. (b) LSC. (c) USEAQ. (d) LearnedS. (e) FS. (f) AFS.

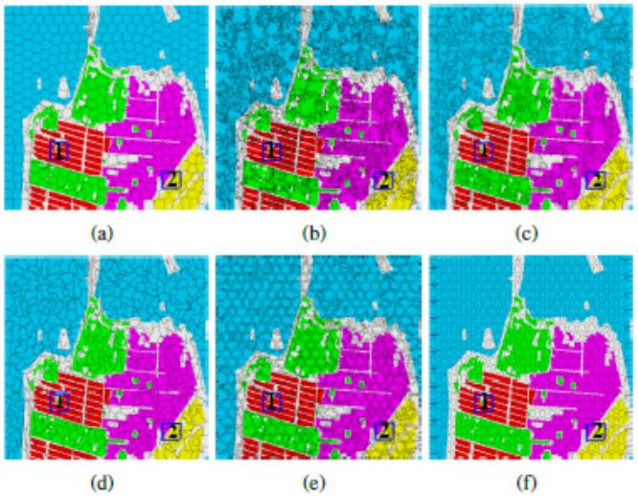

Fig. 17. Comparison of the superpixels segmentations for San Francisco using various methods. (a) SLIC. (b) LSC. (c) USEAQ. (d) LearnedS. (e) FS. (f) AFS.

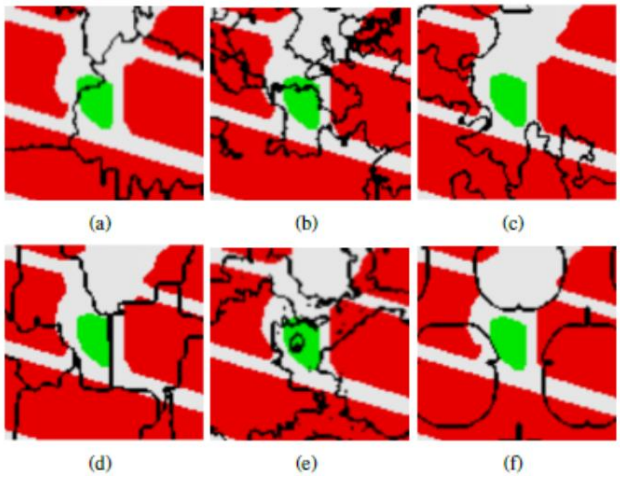

Fig. 18. The enlarged superpixels segmentations of the selected area 1 in San Francisco. (a) SLIC. (b) LSC. (c) USEAQ. (d) LearnedS. (e) FS. (f) AFS.

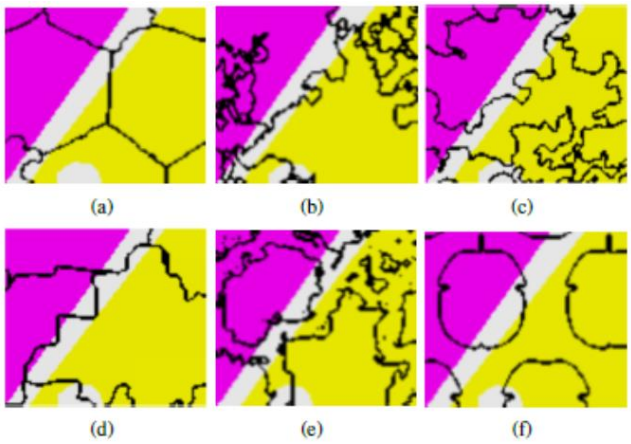

Fig. 19. The enlarged superpixels segmentations of the selected area 2 in San Francisco. (a) SLIC. (b) LSC. (c) USEAQ. (d) LearnedS. (e) FS. (f) AFS.

3) Classification results:

A simple supervised classification process in [34] is used to evaluate the performance of the proposed AFS algorithm. Labeled pixels are firstly selected randomly from superpixels, and all the pixels in any one superpixel are assigned the same label as that of the selected pixels. Each superpixel is then considered as a pre-processed element in classification process. The features of each superpixel are represented by the mean value of the features of all pixels in the superpixel.

In the following experiments, five pixels are selected at random from each class, and the widely used SVM for SAR image classification [38] is chosen as the classifier on images pre-processed with the AFS algorithm. Average accuracy and kappa coefficient of agreement (kappa), both widely used in remote sensing [20], [47], are adopted to evaluate the classification performance quantitatively.

Tables VII, VIII and IX compare the classification accuracy of the six algorithms, where the proposed AFS algorithm shows a better performance. The average classification accuracy of AFS on Flevoland is 89.37%, which is 6.68%, 5.81%, 6.94%, 5.37% and 2.34% higher than SLIC, LSC, USEAQ, LearnedS and FS, respectively. The performance of AFS is nearly the same as those of FS on ESAR with the 1000 and 3000 superpixels. AFS obtained better classification results than the

other algorithms on ESAR, i.e. about 5.69%, 3.80%, 6.27%, 3.90% and 2.18% higher than SLIC, LSC, USEAQ, LearnedS and FS on San Francisco, respectively.

TABLE VII
FLEVOLAND. COMPARISON OF THE CLASSIFICATION RESULTS USING VARIOUS SUPERPIXELS METHODS.

	SLIC	LSC	USEAQ	LearnedS	FS	AFS
200	81.56±6.5	83.86±5.7	81.50±6.6	84.45±7.5	86.70±3.2	**89.64±2.3**
500	83.82±5.3	83.26±2.2	83.36±4.9	83.54±5.2	87.35±1.9	**89.10±2.4**
Mean	82.69	83.56	82.43	84.00	87.03	**89.37**

TABLE VIII
ESAR. COMPARISON OF THE CLASSIFICATION RESULTS USING VARIOUS SUPERPIXELS METHODS.

	SLIC	LSC	USEAQ	LearnedS	FS	AFS
500	62.96±7.7	65.72±8.8	65.21±7.9	67.07±8.2	69.33±5.9	**73.38±5.6**
1000	67.53±7.4	61.50±8.4	64.96±7.5	64.25±7.9	72.77±4.3	**72.93±5.9**
3000	65.27±6.7	64.62±8.0	64.12±8.1	64.24±5.8	**71.25±5.7**	70.41±6.1
Mean	65.25	63.95	64.77	65.19	71.12	**72.24**

TABLE IX
SAN FRANCISCO. COMPARISON OF THE CLASSIFICATION RESULTS USING VARIOUS SUPERPIXELS METHODS.

	SLIC	LSC	USEAQ	LearnedS	FS	AFS
500	81.02±5.0	81.86±5.2	79.28±5.6	83.58±5.1	84.21±3.9	**86.57±3.0**
1000	80.23±5.5	81.61±5.1	79.82±6.3	81.40±5.9	83.59±3.4	**84.91±3.0**
3000	77.87±5.2	81.32±5.0	78.29±4.5	79.52±5.6	81.85±3.4	**84.73±6.1**
Mean	79.71	81.60	79.13	81.50	83.22	**85.40**

Table X shows the kappa values of different algorithms for Flevoland, ESAR and San Francisco with 200, 500 and 500 superpixels, respectively. AFS obtained the highest kappa value, followed by FS.

TABLE X
KAPPA FOR THE THREE IMAGES

	SLIC	LSC	USEAQ	LearnedS	FS	AFS
Flevoland	0.79	0.74	0.73	0.82	0.83	**0.87**
ESAR	0.4	0.36	0.43	0.39	0.50	**0.52**
San Francisco	0.71	0.76	0.65	0.73	0.76	**0.79**

Fig. 20 (a), (b) and (c) shows the classification results of 50 runs on Flevoland with 200 superpixels, ESAR with 500 superpixels and San Francisco with 500 superpixels, respectively. It can be seen that the classification result based on the proposed AFS algorithm again obtained a high accuracy of better stability.

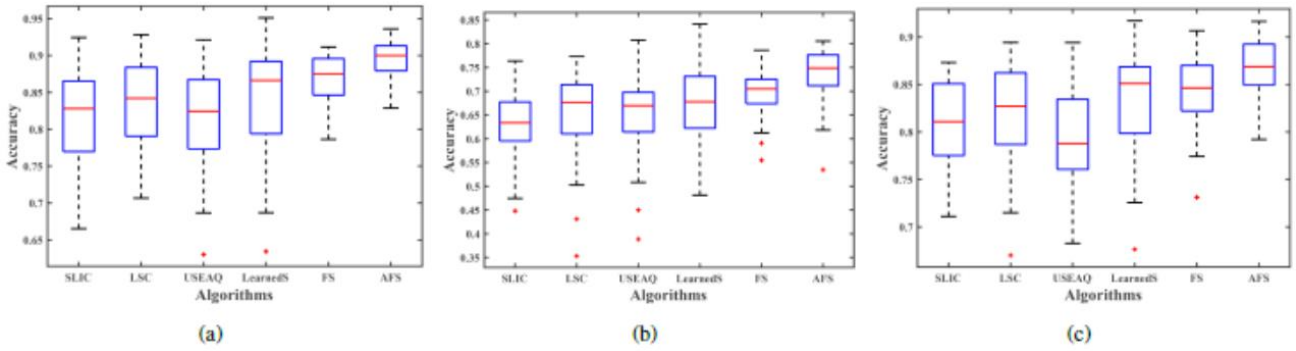

Fig. 20. The accuracy of various methods with running 50. (a) Flevoland. (b) ESAR. (c) San Francisco.

V. CONCLUSIONS

In this paper, a fuzzy superpixels algorithm (AFS) is proposed and evaluated for PolSAR image classification. In AFS, the correlation between polarimetric scattering information is introduced to cluster pixels, which is measured by a fuzzy equivalence relation. This introduced correlation showed to help distinguishing pixels belonging to different classes. Besides, the ratio of undetermined pixels is adjusted adaptively according to the correlation showed to contribute to generating more suitable fuzzy superpixels for different PolSAR image without manual adjustment. Experimental analysis demonstrated the effectiveness of the proposed new AFS applied to three PolSAR images, superior to five state-of-the-art superpixels algorithms.

Region-based classification is an important research topic in PolSAR image processing due to that pixels-based clas-sification algorithms are sensitive to speckle noise and of high complexity. In this paper, we use a simple classifica¬tion process, focusing on designing a superpixels model for image classification and evaluating the performance of AFS. In the future work, we plan to develop and combine a specific classification process with the AFS algorithm for more accurate PolSAR image classification.

REFERENCES

[1] X. Ren and J. Malik, “Learning a classification model for segmentation,” in *IEEE International Conference on Computer Vision, 2003. Proceedings*, 2003, pp. 10–17.

[2] W. Zhao, L. Jiao, W. Ma, J. Zhao, J. Zhao, H. Liu, X. Cao, and S. Yang, “Superpixel-based multiple local cnn for panchromatic and multispectral image classification,” *IEEE Transactions on Geoscience and Remote Sensing*, vol. 55, no. 7, pp. 4141–4156, 2017.

[3] S. Jia, B. Deng, J. Zhu, X. Jia, and Q. Li, “Superpixel-based multitask learning framework for hyperspectral image classification,” *IEEE Transactions on Geoscience and Remote Sensing*, vol. PP, no. 99, pp. 1–14, 2017.

[4] T. Liu, Y. Gu, J. Chanussot, and M. D. Mura, “Multimorphological superpixel model for hyperspectral image classification,” *IEEE Transactions on Geoscience and Remote Sensing*, vol. PP, no. 99, pp. 1–14, 2017.

[5] T. H. Dang, D. S. Mai, and L. T. Ngo, “Multiple kernel collaborative fuzzy clustering algorithm with weighted super-pixels for satellite image land-cover classification,” *Engineering Applications of Artificial Intelligence*, vol. 85, pp. 85–98, 2019.

[6] Z. Fu, Y. Sun, L. Fan, and Y. Han, “Multiscale and multifeature segmentation of high-spatial resolution remote sensing images using superpixels with mutual optimal strategy,” *Remote Sensing*, vol. 10, no. 8, p. 1289, 2018.

[7] B. Sheng, P. Li, S. Mo, H. Li, X. Hou, Q. Wu, J. Qin, R. Fang, and D. D. Feng, "Retinal vessel segmentation using minimum spanning superpixel tree detector," *IEEE transactions on cybernetics*, vol. 49, no. 7, pp. 2707–2719, 2018.

[8] J. Yang, Z. Gan, K. Li, and C. Hou, "Graph-based segmentation for rgb-d data using 3-d geometry enhanced superpixels," *IEEE transactions on cybernetics*, vol. 45, no. 5, pp. 927–940, 2014.

[9] Y.-F. Wang, H.-M. Liu, and Z.-W. Fu, "Low-light image enhancement via the absorption light scattering model," *IEEE Transactions on Image Processing*, vol. 28, no. 11, pp. 5679–5690, 2019.

[10] X. Li, K. Liu, and Y. Dong, "Superpixel-based foreground extraction with fast adaptive trimaps." *IEEE Transactions on Cybernetics*, vol. PP, no. 99, pp. 1–11, 2017.

[11] M. Chen, X. Wei, Q. Yang, Q. Li, G. Wang, and M. H. Yang, "Spatiotem-poral gmm for background subtraction with superpixel hierarchy," *IEEE Transactions on Pattern Analysis and Machine Intelligence*, vol. PP, no. 99, pp. 1–1, 2017.

[12] W. Fang, T. Zhang, C. Zhao, D. B. Soomro, R. Taj, and H. Hu, "Background subtraction based on random superpixels under multiple scales for video analytics," *IEEE Access*, vol. 6, pp. 33376–33386, 2018.

[13] X. Zhou, X. Li, and W. Hu, "Learning a superpixel-driven speed function for level set tracking," *IEEE transactions on cybernetics*, vol. 46, no. 7, pp. 1498–1510, 2015.

[14] L. Wang, H. Lu, and M. H. Yang, "Constrained superpixel tracking." *IEEE Transactions on Cybernetics*, vol. PP, no. 99, pp. 1–12, 2017.

[15] M. Shen, Y. Zhang, R. Wang, J. Yang, L. Xue, and M. Hu, "Robust object tracking via superpixels and keypoints," *Multimedia Tools and Applications*, vol. 77, no. 19, pp. 25 109–25 129, 2018.

[16] Q. Wang, J. Lin, and Y. Yuan, "Salient band selection for hyperspectral image classification via manifold ranking," *IEEE transactions on neural networks and learning systems*, vol. 27, no. 6, pp. 1279–1289, 2016.

[17] Q. Wang, X. He, and X. Li, "Locality and structure regularized low rank representation for hyperspectral image classification," *IEEE Transactions on Geoscience and Remote Sensing*, vol. 57, no. 2, pp. 911–923, 2018.

[18] X. Zhang, J. Xia, X. Tan, X. Zhou, and T. Wang, "Polsar image classification via learned superpixels and qcnn integrating color features," *Remote Sensing*, vol. 11, no. 15, p. 1831, 2019.

[19] B. Hou, C. Yang, B. Ren, and L. Jiao, "Decomposition-feature-iterative-clustering-based superpixel segmentation for polsar image classifica tion," *IEEE Geoscience and Remote Sensing Letters*, vol. 15, no. 8, pp. 1239–1243, 2018.

[20] Y. Li, R. Xing, L. Jiao, Y. Chen, Y. Chai, N. Marturi, and R. Shang, "Semi-supervised polsar image classification based on self-training and superpixels," *Remote Sensing*, vol. 11, no. 16, p. 1933, 2019.

[21] J. Li, H. Zhang, and L. Zhang, "Efficient superpixel-level multitask joint sparse representation for hyperspectral image classification," *IEEE Transactions on Geoscience and Remote Sensing*, vol. 53, no. 10, pp. 5338–5351, 2015.

[22] H. Tong, F. Tong, W. Zhou, and Y. Zhang, "Purifying slic superpixels to optimize superpixel-based classification of high spatial resolution remote sensing image," *Remote Sensing*, vol. 11, no. 22, p. 2627, 2019.

[23] G. K¨orner, D. Oppelt, J. Adametz, and M. Vossiek, "Novel passive calibration method for fully polarimetric near field mimo imaging radars," in *2019 12th German Microwave Conference (GeMiC)*. IEEE, 2019, pp. 150–153.

[24] S.-q. Huang and D.-z. Liu, "Some uncertain factor analysis and improvement in spaceborne synthetic aperture radar imaging," *Signal processing*, vol. 87, no. 12, pp. 3202–3217, 2007.

[25] Z. Pawlak, "Rough sets," *International journal of computer & information sciences*, vol. 11, no. 5, pp. 341–356, 1982.

[26] D. Dubois and H. Prade, "Rough fuzzy sets and fuzzy rough sets," *International Journal of General System*, vol. 17, no. 2-3, pp. 191–209, 1990.

[27] J. Dai and Q. Xu, "Attribute selection based on information gain ratio in fuzzy rough set theory with application to tumor classification," *Applied Soft Computing*, vol. 13, no. 1, pp. 211–221, 2013.

[28] J. Shi and J. Malik, "Normalized cuts and image segmentation," *IEEE Transactions on Pattern Analysis and Machine Intelligence*, vol. 22, no. 8, pp. 888–905, 2000.

[29] R. Achanta, A. Shaji, K. Smith, A. Lucchi, and P. Fua, "Slic superpixels compared to state-of-the-art superpixel methods," *IEEE Transactions on Pattern Analysis and Machine Intelligence*, vol. 34, no. 11, pp. 2274– 2282, 2012.

[30] Z. Li and J. Chen, "Superpixel segmentation using linear spectral clustering," in *Proceedings of the IEEE Conference on Computer Vision and Pattern Recognition*, 2015, pp. 1356–1363.

[31] Y. J. Liu, M. Yu, B. J. Li, and Y. He, "Intrinsic manifold slic: A simple and efficient method for computing content-sensitive superpixels," *IEEE Transactions on Pattern Analysis and Machine Intelligence*, vol. PP, no. 99, pp. 1–1, 2017.

[32] C.-R. Huang, W.-C. Wang, W.-A. Wang, S.-Y. Lin, and Y.-Y. Lin, "Useaq: Ultra-fast superpixel extraction via adaptive sampling from quantized regions," *IEEE Transactions on Image Processing*, vol. 27, no. 10, pp. 4916–4931, 2018.

[33] W.-C. Tu, M.-Y. Liu, V. Jampani, D. Sun, S.-Y. Chien, M.-H. Yang, and J. Kautz, "Learning superpixels with segmentation-aware affinity loss," in *Proceedings of the IEEE Conference on Computer Vision and Pattern Recognition*, 2018, pp. 568–576.

[34] Y. Guo, L. Jiao, S. Wang, S. Wang, F. Liu, and W. Hua, "Fuzzy super-pixels for polarimetric sar images classification," *IEEE Transactions on Fuzzy Systems*, vol. 26, no. 5, pp. 2846–2860, 2018.

[35] C. Yang, B. Hou, B. Ren, Y. Hu, and L. Jiao, "Cnn-based polarimetric decomposition feature selection for polsar image classification," *IEEE Transactions on Geoscience and Remote Sensing*, 2019.

[36] J. C. Bezdek, R. Ehrlich, and W. Full, "Fcm: The fuzzy c-means clustering algorithm," *Computers & Geosciences*, vol. 10, no. 2-3, pp. 191–203, 1984.

[37] F. H¨oppner, F. Klawonn, R. Kruse, and T. Runkler, *Fuzzy cluster analysis: methods for classification, data analysis and image recognition*. John Wiley & Sons, 1999.

[38] S. Uhlmann and S. Kiranyaz, "Integrating color features in polarimetric sar image classification," *IEEE Transactions on Geoscience and Remote Sensing*, vol. 52, no. 4, pp. 2197–2216, 2013.

[39] J. C. Bezdek, *Pattern recognition with fuzzy objective function algorithms*. Springer Science & Business Media, 2013.

[40] A. Yu, P. Qin, "Unsupervised polarimetric sar image segmentation and classification using region growing with edge penalty," *IEEE Transactions on Geoscience and Remote Sensing*, vol. 50, no. 4, pp. 1302–1317, 2012.

[41] B. Liu, H. Hu, H. Wang, and K. Wang, "Superpixel-based classification with an adaptive number of classes for polarimetric sar images," *IEEE Transactions on Geoscience and Remote Sensing*, vol. 51, no. 2, pp. 907–924, 2013.

[42] S. Uhlmann and S. Kiranyaz, "Integrating color features in polarimetric sar image classification," *IEEE Transactions on Geoscience and Remote Sensing*, vol. 52, no. 4, pp. 2197–2216, 2014.

[43] B. Liu, H. Hu, H. Wang, K. Wang, X. Liu, and W. Yu, "Superpixel-based classification with an adaptive number of classes for polarimetric sar images," *IEEE Transactions on Geoscience and Remote Sensing*, vol. 51, no. 2, pp. 907–924, 2012.

[44] N. Zhong, W. Yang, A. Cherian, X. Yang, G. S. Xia, and M. Liao, "Unsupervised classification of polarimetric sar images via riemannian sparse coding," *IEEE Transactions on Geoscience and Remote Sensing*, vol. PP, no. 99, pp. 1–10, 2017.

[45] F. Liu, L. Jiao, and X. Tang, “Task-oriented gan for polsar image classification and clustering,” *IEEE transactions on neural networks and learning systems*, vol. 30, no. 9, pp. 2707–2719, 2019.

[46] M. Van den Bergh, X. Boix, G. Roig, and L. Van Gool, “Seeds: Superpixels extracted via energy-driven sampling,” *International Journal of Computer Vision*, vol. 111, no. 3, pp. 298–314, 2015.

[47] W. D. Hudson, “Correct formulation of the kappa coefficient of agreement,” *Photogrammetric engineering and remote sensing*, vol. 53, no. 4, pp. 421–422, 1987.

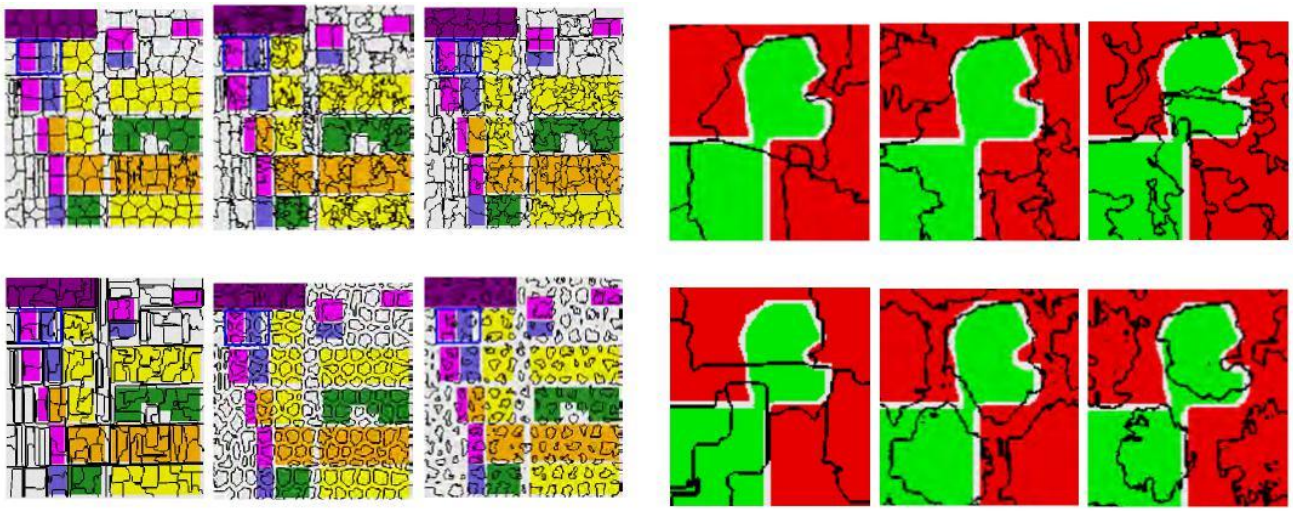
1
2

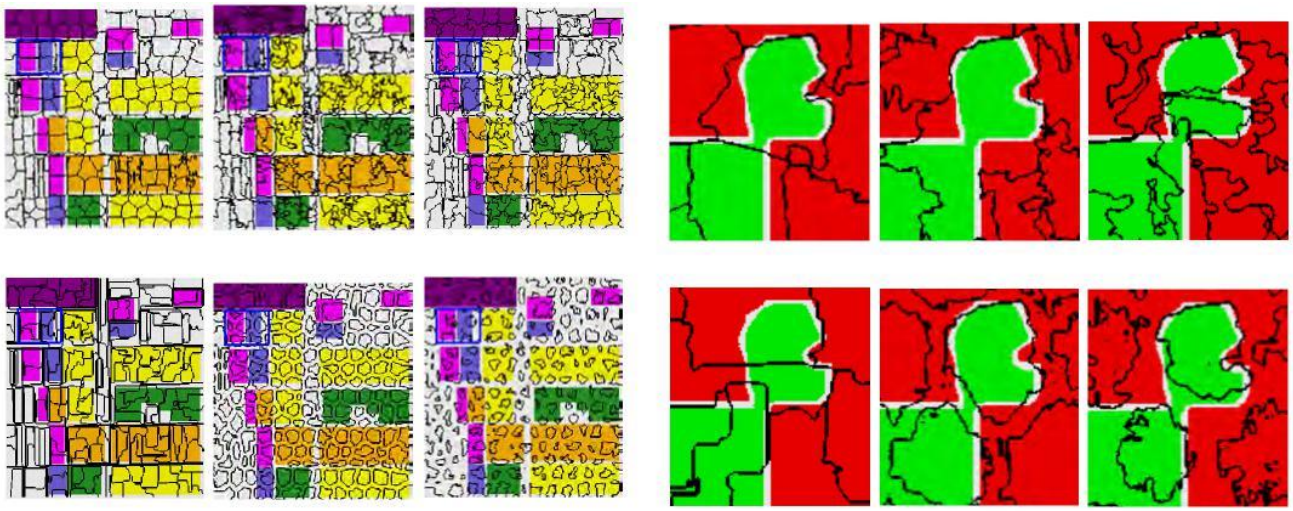
1
2

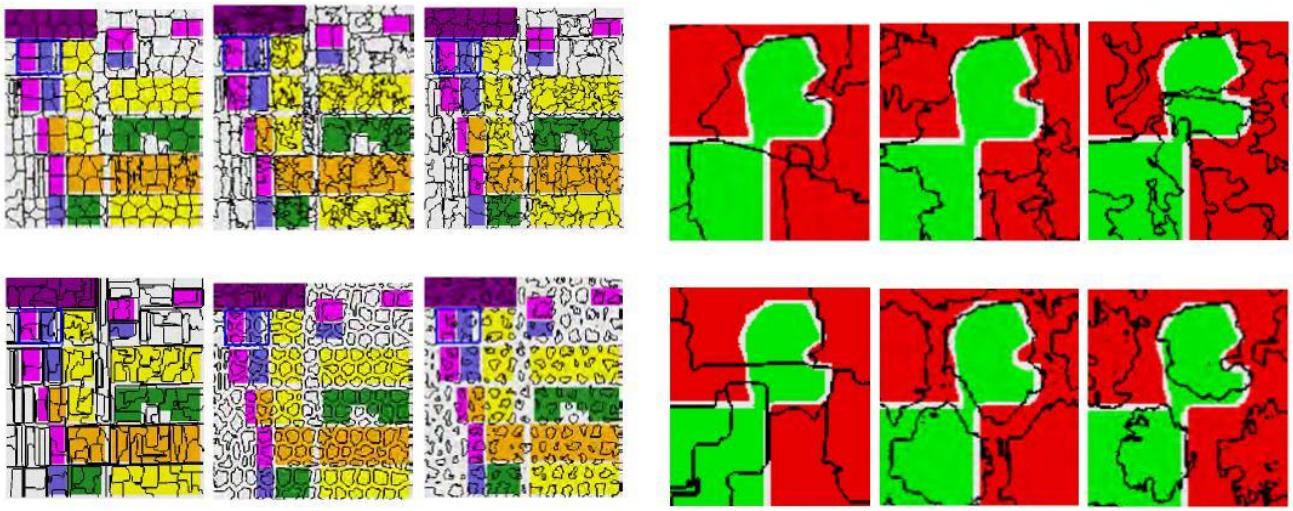
1
2

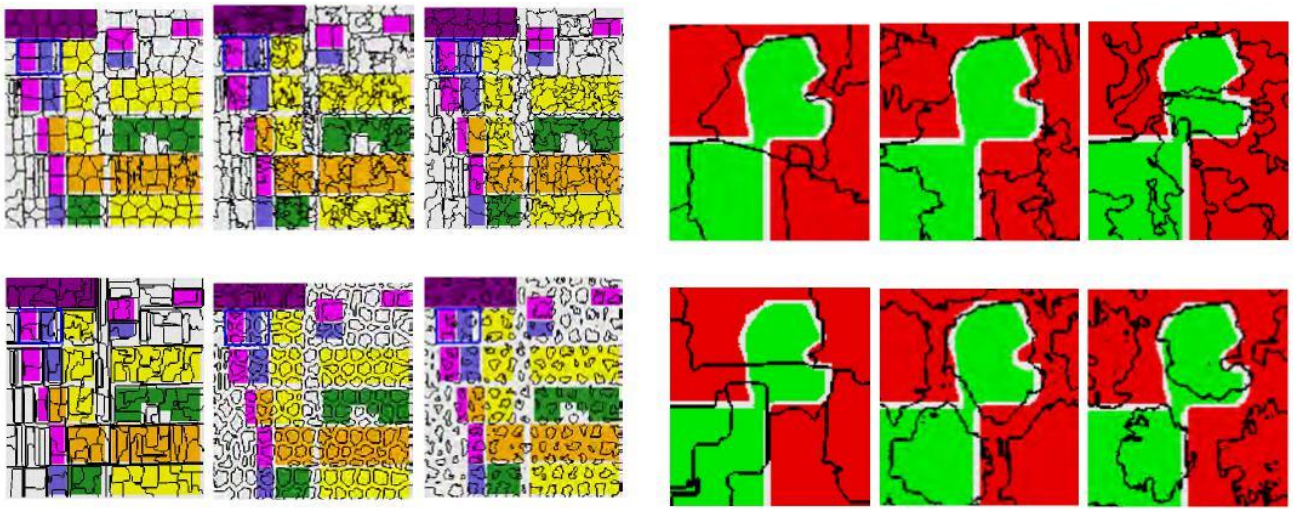
1
2